Numerical Simulation of the Wire-Pinning Process in PET Film Casting: Steady-State Results

Kostas Christodoulou
Avery-Dennison Research Center, 2900 Bradley Street, Pasadena, CA 91107-1599

Savvas G. Hatzikiriakos
Dept. of Chemical and Biological Engineering, The University of British Columbia, 2216 Main Mall, Vancouver, BC, Canada V6T-1Z4

Evan Mitsoulis
School of Mining Engineering and Metallurgy, National Technical University of Athens, 157 80 Zografou, Athens, Greece

DOI 10.1002/aic.12734
Published online August 16, 2011 in Wiley Online Library (wileyonlinelibrary.com).

Poly(ethylene terephthalate) (PET) film casting involves melt flow through a slot die, across a small span, and onto a fast moving quench drum. In the ''wire-pinning'' casting process, a thin electrified wire close to the line of contact with the drum creates a strong pinning force that delays air entrainment to higher line speeds. Nonuniform wetting of the die lips by the extruded melt is thought to be responsible for the formation of streaks, a defect in the machine direction. A finite element model of the film casting process with wire pinning was developed to assist in understanding what causes significant wetting of the lips and whether this can be avoided by electrostatic pinning. The solution of the governing equations provide the location of the static and dynamic contact lines, thus finding the wetting and pinning points in the process. The simulations investigate the sensitivity of the static wetting line locations on the die lands to the imposed values of static contact angle and die-lip gap. It was found that while the contact angle has a small effect on the extent of die-lip wetting within the parameter ranges examined, there is a considerable chance that the feed slot surfaces can be dewetted. This seems to be the greatest danger for causing streaks rather than excessive wetting of the die lands. © 2011 American Institute of Chemical Engineers *AIChE J,* 58: 1979–1986, 2012

Keywords: film casting, film pinning, PET resins, finite element model, wetting of die lip

Introduction

Die casting of poly(ethylene terephthalate) (PET) film involves polymer melt flow through a slot die, across a short gap as a free liquid curtain, and onto a revolving quench drum where the melt solidifies into a thermoplastic film (see Figure 1). In the absence of any pinning forces, the high-melt viscosity causes the liquid curtain to be pulled downstream by the drum resulting in a long effective casting span. Consequently, there is a liquid curtain neck-in at the edges, which gives rise to a nonuniform thickness and polymer orientation profiles with a characteristic ''dog-bone'' shape in the cross-machine direction.[1]

Another problem encountered in film casting is nonuniform wetting of the die lips by the extruded melt, which is thought to be responsible for the formation of ''streaks,'' a defect in the machine direction which persists in the final film. Other relevant process problems include flow instabilities, such as draw resonance and edge weave, which give rise to spontaneous thickness and width oscillations.[2–5]

To avoid many of these undesirable effects, a pinning force is often used that facilitates contact between the melt curtain and the quench drum. Examples of pinning forces include: (a) a pressure differential (vacuum) across the liquid curtain; (b) a positive pressure field applied by an ''air knife'' on the upper surface; (c) an electrostatic field by an electrical wire placed close to the desired contact line location; or (d) combinations of these (see Figure 1).[6,7]

In electrostatic pinning, which is the main focus of this work, a high voltage (of the order of 6–8 kV) is applied on the wire, whereas the drum is maintained at ground potential. As a result, ions migrate toward the molten portion of the film and are trapped at its solidification front. The potential difference between the film and the drum creates a strong local force that pins the film onto the roll surface. This pinning process reduces neck-in and improves thickness uniformity and heat transfer. It may also affect the wetting of the die lips by the melt and thus affect streak formation.

To investigate the possibility of reducing lip wetting and therefore streak formation by means of wire pinning, a finite element model of PET film casting flow was developed.

Correspondence concerning this article should be addressed to K. Christodoulou at Kostas.Christodoulou@averydennison.com.

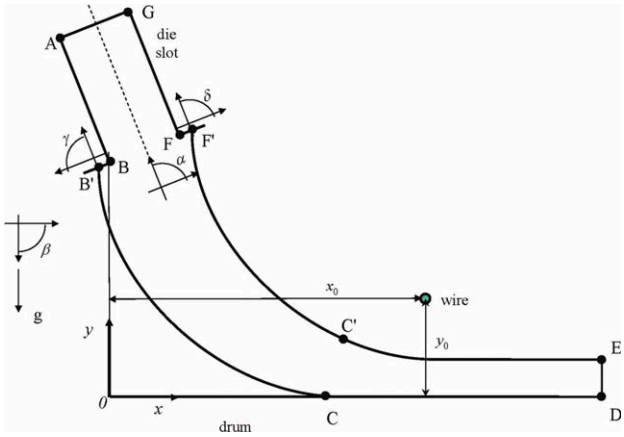

Figure 1. Schematic of the wire-pinning casting process.

[Color figure can be viewed in the online issue, which is available at wileyonlinelibrary.com.]

The goal is to ultimately predict the formation of such defects or at least the conditions under which significant wetting of the lips is prevented and thereby extend the parameter range of defect-free operation, the so-called "process operability window." But to do this, first a full analysis of the process is required, which will highlight the relevant parameters at work and the interaction of several of these in the process.

The film casting model developed in this work is based on the general model of free surface flows reported previously by Christodoulou et al.[8] A predictive model requires a constitutive relation that adequately describes the rheological response of the melt at the shear and extension rates of the process. As PET shows a Newtonian behavior for an extended range of shear rates,[9,10] a Newtonian isothermal fluid is considered in this work, as a first approximation before viscoelastic effects are taken into account, a task much more demanding. The electrostatic force due to the wire is included through a semitheoretical equation that is justified and discussed in detail below. Solutions will be found by running steady-state calculations for several sets of parameters.

In summary, the model developed here will be used to determine: (a) the pinning location of the film on the drum as a function of the electrostatic pinning force location and strength; and (b) the locations of the static and dynamic contact lines, where the melt leaves the die and where it first contacts the casting drum, respectively.

Mathematical Modeling

We consider the flow of a PET melt through a slot die, across a small gap and onto a fast moving quench drum (Figure 1). The flow in the casting span is predominantly extensional and would normally cause the melt bridge to neck in laterally.[1] This neck-in increases with the length of the span. When the casting span is short, which is common in the actual process, two simplifications occur. First, neck-in is small and can be safely neglected, leading to a transversely uniform, two-dimensional (2-D) flow, except for unavoidable edge effects. Second, the flow is isothermal up to the contact of the melt with the quench drum. Even beyond this point, the flow relaxes fast to plug flow, and nonisothermal effects are often inconsequential.[11–14]

The flow of a viscous melt is governed by the usual set of conservation and constitutive equations. The mass and momentum conservation equations for incompressible isothermal steady-state flow are:

$$\nabla \cdot \bar{\mathbf{v}} = 0, \tag{1}$$

$$\rho \bar{\mathbf{v}} \cdot \nabla \bar{\mathbf{v}} = -\nabla p + \nabla \cdot \bar{\bar{\tau}} + \rho \bar{\mathbf{g}}, \tag{2}$$

where $\bar{\mathbf{v}}$ is the velocity vector, ρ is the melt density, p is the scalar isotropic pressure, $\bar{\bar{\tau}}$ is the extra-stress tensor, and $\bar{\mathbf{g}}$ is the acceleration of gravity vector acting downward. Although steady flows of interest here are of very low Reynolds numbers, the inertial terms in the momentum Eq. 2 are kept for completion. The set of Eqs. 1–2 is closed by a constitutive law for the extra stresses, $\bar{\bar{\tau}}$. A Newtonian behavior is assumed here, which is a good approximation for PET, as far as viscous behavior is concerned (elastic effects are expected to be important but are not addressed in this work) as shown in Figure 2 for a wide range of shear rates (<10 s^{-1}):[9,10]

$$\bar{\bar{\tau}} = \mu \bar{\bar{\dot{\gamma}}}. \tag{3}$$

Here, $\bar{\bar{\dot{\gamma}}}$ is the rate-of-strain tensor defined as $\bar{\bar{\dot{\gamma}}} \equiv \nabla \bar{\mathbf{v}} + (\nabla \bar{\mathbf{v}})^T$, and μ is the Newtonian viscosity.

The system of equations becomes dimensionless by using a characteristic length H (here taken as the die-lip opening H_0) and a characteristic velocity U (here taken as the die entry mean velocity V_d). Then the dimensionless numbers are the Reynolds number, Re, and Stokes number, St, defined by:

$$\mathrm{Re} = \frac{\rho V_d H_0}{\mu}, \tag{4}$$

$$\mathrm{St} = \frac{\rho g H_0^2}{\mu V_d}, \tag{5}$$

The system of equations can only be solved when a set of appropriate boundary conditions is imposed along the domain perimeter. In the present case, these are the following (see Figure 1):

(a) along the solid die walls AB and GF, the velocity was specified as zero (no-slip condition) $\bar{\mathbf{v}} = 0$;

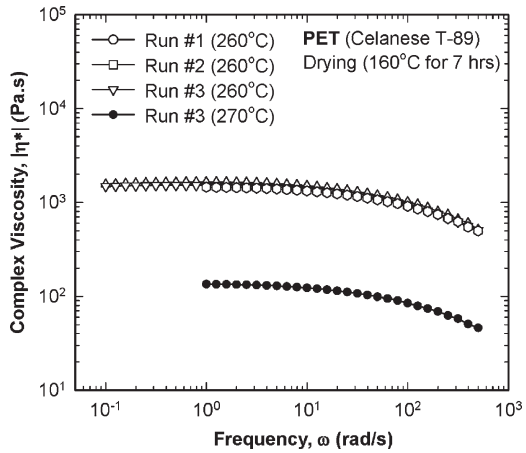

Figure 2. Shear viscosity of PET showing a Newtonian behavior in the low range of shear rates (<10 s^{-1}).

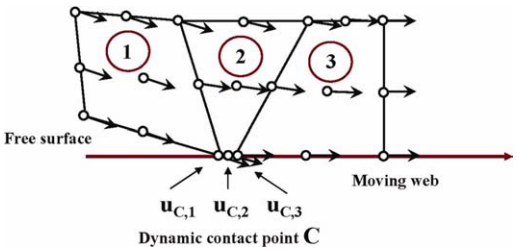

Figure 3. Modeling of the dynamic contact line with collapsed finite elements.

Nodes C1, C2, and C3 have the same coordinates but different velocities. [Color figure can be viewed in the online issue, which is available at wileyonlinelibrary.com.]

(b) along the moving drum (or web) CD, no slip condition was imposed with the velocity of the melt equal to the velocity of the web $\bar{\mathbf{v}} = V_w$;

(c) along the inflow boundary GA, placed sufficiently far upstream in the die-slot (see below), a parabolic velocity profile was specified;

(d) along the outflow boundary DE, located on the quench drum sufficiently far downstream of the contact point C (see below), a plug velocity profile and the slope of the free surface were specified;

(e) along the two free surfaces B′C and F′E, the conditions used were no melt penetration (kinematic equation), vanishing air friction and viscous forces balancing capillary and external pressures, i.e.,

$$\bar{\mathbf{n}} \cdot \bar{\mathbf{v}} = 0, \tag{6}$$

$$\bar{\mathbf{n}} \cdot \bar{\mathbf{T}} = \left(\frac{2H}{\mathrm{Ca}} + p_a \right) \bar{\mathbf{n}} \, . \tag{7}$$

Here, $\bar{\mathbf{n}}$ is the local unit normal vector to the free boundary; $2H \equiv -\nabla_{II} \cdot \mathbf{n}$ is the mean curvature of the free surface, ∇_{II} is the gradient operator on a surface;[15] and p_a is the ambient pressure. The capillary number Ca is given by:

$$\mathrm{Ca} = \frac{\mu V_d}{\sigma}, \tag{8}$$

where σ is the surface tension of the melt.

(f) at the dynamic contact line (point C), where the melt first contacts the quench drum, the velocity field was made multivalued (discontinuous) by collapsing the quench-drum side of the finite element there into one point (in the real x–y domain while keeping three distinct nodes in the isoparametric domain). This procedure creates a singular element, which allows the imposition of the proper kinematic conditions on both the free surface side of the element upstream of the contact line and on the quench-drum side of the element downstream of the contact line. Other, more elaborate choices are possible and discussed elsewhere.[8] The angle of contact of the liquid/air interface with the moving substrate surface was not specified there but instead the kinematic condition (Eq. 4) was kept as the additional equation associated with the contact line location. This procedure only works at high capillary numbers (Ca >> 1), i.e., for negligible surface tension and very high viscosity, which are common in melt flows such as the ones studied here.

(g) At the two static wetting lines at the exit of the die slot (points B and F), where the melt/air interfaces meet the stationary die lands, Gibbs' complementary condition was used:[8]

$$(\theta_S - \theta) h_S = 0, \tag{9a}$$

$$h_s \geq 0, \quad \theta_s - \theta \geq 0, \tag{9b}$$

where $\theta \equiv \cos^{-1}(\mathbf{n} \cdot \mathbf{n}_s)$ and $\theta_S \equiv \cos^{-1}(\mathbf{n}_s \cdot \mathbf{n}_s)$ is the static contact angle, and $\mathbf{n}_s$ is the unit normal to the solid surface; h_S is the wet length from the die corner to the contact line (BB′ and FF′); θ_S can be regarded as an empirical parameter that must be inferred from experiments.

It should be noted that Gibbs' complementary condition allows for the finding of lip wetting, namely the points outside the die where the extruded melt detaches from the die. These two points, which in principle are not symmetric, are thought to be responsible for the development of "streaks," which are detrimental for the final product.

Method of Solution

The finite element formulation used is fully documented elsewhere[8] and will not be repeated here. The model can predict the transversely uniform (2-D) steady slot-curtain flow. A few other highlights of the present model that are not shared by any commercial codes are described next.

Treatment of static and dynamic contact points

The physics of the contact lines is still not fully understood. It is well known that stress singularities arise there. At static contact lines, where the melt separates from static solid surfaces the singularity is rather mild. In this study at the static contact lines, the (static) contact angle θ_S between the melt and die surface was specified. The wet length h_S is usually a strong function of this contact angle.

However, at dynamic wetting lines, the singularity is so strong as to be nonintegrable even for a Newtonian fluid. Obviously, other physics at the microscopic scale act to relieve such strong singularities. To alleviate those and make them integrable, a slip region is usually used in the vicinity of the contact line, in which the velocity of the liquid lags that of the solid by an amount proportional to the local shear stress. This "slip" method, however, gives rise to nonphysical artifacts, such as deceleration of the liquid approaching the contact line.

Instead, here we use the technique of "singular elements," first introduced in fracture mechanics to capture singular stresses at crack tips.[16] In this method, one side of the element adjacent to the contact line is collapsed creating a "triple" node there (see Figure 3). The collapsing is effected by a penalty term to the mesh generation equations that specifies that mesh size is zero for that element side. The resulting extra degrees of freedom at the contact line allow specification of both the kinematic condition at the free surface side and the no-slip condition on the drum side and give rise to the apparent discontinuous velocity there. The kinematic singularity is accurately captured in this way, without polluting the macroscopic flow field with non-physical oscillations ("wiggles"). Still the dynamic contact angle θ_d is a required parameter that lumps the microscopic physics of the three-phase interaction there.

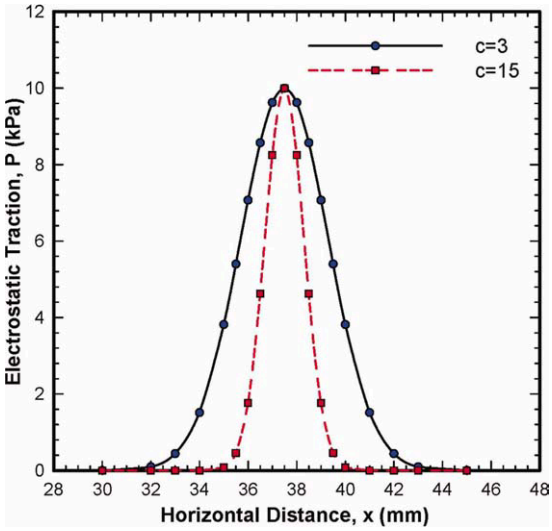

Figure 4. Electrostatic traction vs horizontal distance assumed to follow a Gaussian distribution (Eq. 10).

[Color figure can be viewed in the online issue, which is available at wileyonlinelibrary.com.]

Pinning force

Electrostatic pinning is a technology used to improve the intimacy of contact of an extruded polymer melt onto a casting wheel in the process of producing films.[17] To predict the pinning force due to the electrified wire, a complex 2-D electrostatics problem would have to be solved together with the free-surface flow problem, as the two are coupled. Here, the pinning force of the wire was approximated from experience as an attractive traction between the lower free surface of the melt curtain and the drum (see Figure 1). This traction was taken to be a Gaussian function only of the horizontal distance x from the wire (Figure 4). Its maximum, P_{max}, was taken to be 10 kPa at the horizontal location of the wire $x_0 = 37.5$ mm, going down to 0 kPa at $x = 30$ mm:

$$P = P_{max} \exp\left[-\frac{c}{2}\left(\frac{x - x_0}{L_0}\right)^2\right], \qquad (10)$$

where $L_0 = 3.12$ mm is the unit of length, equal to the die-lip opening H_0; c determines the rate of decay of the electrostatic field away from the maximum. Here, the value $c = 15$ was used for a sharp curtain drop and $c = 3$ for a smoother curtain drop.

Finite element discretization

The conservation and constitutive equations together with the boundary conditions were discretized by means of the Galerkin finite element method (G-FEM). The elliptic mesh generation scheme developed by Christodoulou and Scriven[18] was used to generate an adaptive mesh that automatically follows the free surfaces as they deform. It solves a pair of partial differential equations for the coordinates, which optimize the orthogonality, smoothness, and concentration of the mesh points to minimize the discretization error. The result of the full discretization of the governing equations is a set of ordinary differential and algebraic equations for the vector of nodal unknowns (velocities, pressures, and positions, *u-v-p-x-y* formulation). The steady 2-D state of this equation set at the parameter set of interest was computed by a full Newton–Raphson iteration and a higher-order continuation scheme (see below). The starting point was a steady state corresponding to a vacuum pinning process without electrostatic assist. The parameter values of the base state are given in Table 1.

Table 1. Parameter Values of Case s-s #1

Parameters	Symbol	Base value
Cast film thickness	H_1	1.68 mm
Die-lip opening	H_0	3.12 mm
Die-to-drum vertical distance	d	16 mm
Pinning-wire to die exit horizontal distance	d_w	37.5 mm
Drum speed	V_w	0.208 m s^{-1}
Die entry mean velocity	V_d	0.112 m s^{-1}
Maximum electrostatic traction	P_{max}	10 kPa
Viscosity	μ	135 Pa s
Density	ρ	1200 kg m^{-3}
Surface tension	σ	20 mN m^{-1}
Dynamic contact angle	θ_d	179.9°
Upstream die static contact angle	θ_{S1}	20°
Downstream die static contact angle	θ_{S2}	20°
Slot-drum angle	α	90°
Drum-gravity angle	β	−90°
Die cutback angle 1	δ	90°
Die cutback angle 2	γ	90°

Various finite element meshes of increasing refinement were used. The main runs were made on a mesh consisting of 1020 elements (Mesh 1) distributed in five different zones, which are necessary to take into account probable wetting of the die lips by the melt. Figure 5 shows these five zones. They are: (1) slot (ABFG), (2) lower part of curtain (including the wet length on the die lip) (BB′CM), (3) drum (CDEC′), (4) body of curtain (BMNF), and (5) upper part of curtain (including the wet length on the die lip) (FNC′F′). The number of elements NE used in each zone is shown in Table 2 and is made up of the number of elements in the x-direction NE_x and in the y-direction NE_y ($NE = NE_x \times Ne_y$). Test runs were made on Mesh 2 having four times the number of elements of M1 and showed no discernible differences from the results with M2. This is not surprising because the fluid considered here is Newtonian and the results do not depend much on grid refinement for Newtonian fluids, as evidenced in the Newtonian extrudate swell case.[19]

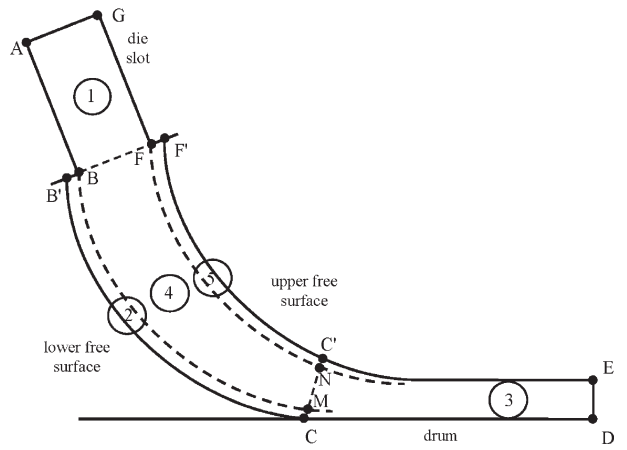

Figure 5. Finite element zones (super-elements) in which the solution domain is subdivided.

Table 2. Mesh Parameters for Meshes M1 and M2

	Mesh M1			Mesh M2		
Zones	NE_x	NE_y	NE	NE_x	NE_y	NE
1	20	6	120	40	12	480
2	80	2	160	160	4	640
3	20	9	180	40	18	720
4	80	6	480	160	12	1920
5	80	1	80	160	2	320
Total # of elements:			1020			4080

The upstream entry length AB and the downstream exit length CD were given sufficient distances as to allow the imposition of fully developed velocity profiles at inlet and outlet. Using the die gap (H_0) as a characteristic length, the entry length was set at $2H_0$ and the exit length at $4H_0$. As mentioned above, because the fluids considered here are Newtonian, these lengths were found adequate (no viscoelasticity present with long-time memory effects requiring a longer computational domain).[20]

Results and Discussion

Horizontal flat substrate

Figure 1 shows a schematic of the die casting system. Horizontal distances are measured from the left side of the die slot (point B). The die lips have been assumed to end into sharp rather than rounded corners. The first steady state (s-s #1) was calculated assuming casting onto a flat horizontal substrate, whereas in the second case, we will take into account the slope of the round drum at the touchdown line. For this case, the dimensionless parameters are: Re = 0.003, Ca = 756, St = 0.008. These numbers indicate that inertia and surface tension effects are not very important (very viscous flows), while gravity does play a role in the domain at hand.

Figure 6a shows the free surface profile and finite element mesh of the computed s-s #1 at the base parameter set of Table 1. The main feature of this flow is a slight inflection point on the liquid curtain around the middle of its length. With the sharply dropping electrostatic force ($c = 15$ in Eq. 10), the dynamic contact line pins at a location of $x_C = 36.85$ mm from the die exit (the x-axis origin is at the upstream slot tip). This is close to the x-coordinate of the electrostatic wire, $x_0 = 37.5$ mm. With the smoother dropping force ($c = 3$), the dynamic contact point pins at $x_C = 34.9$ mm. Below it is found that a much smaller traction than specified is adequate in pinning the contact point, although at a slightly displaced location downstream.

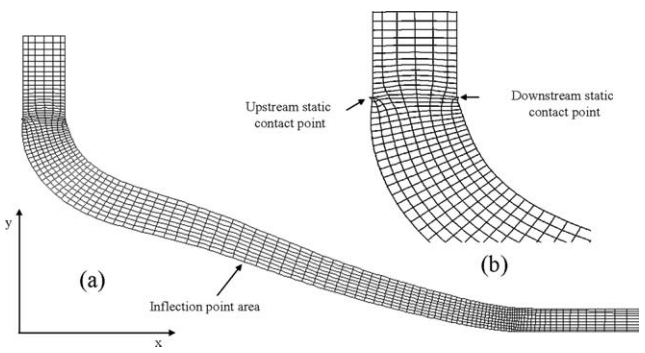

Figure 6. Finite element mesh of computed steady case of the horizontal flat substrate (s-s #1).

(a) Full domain; (b) detail in the die exit region.

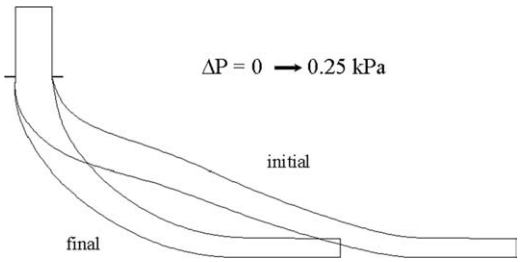

Figure 7. Initial and final free surface profiles from time integration after imposing a vacuum of 0.25 kPa in s-s #1.

The locations of the two static contact lines on the die lips are also predicted by the analysis. Figure 6b shows a magnified view of the mesh in the region of the slot exit so that the wet lengths can be seen. Under the given conditions and with static contact angles on the die surfaces of 20°, the upstream wet length h_S is predicted to be 0.124 mm and the downstream one 0.0722 mm; therefore, a distinctly nonuniform lip-wetting phenomenon occurs. (The postprocessor FIPOST[21] used to produce these plots, substitutes the quadratic functions used for the free-surface parameterization with piece-wise linear functions, which explains the apparent contact angles that seem greater than 20°). Evidently, there is very little wetting of the lips, probably due to the high melt viscosity and the extension of the melt curtain by the drum, causing a contraction in the thickness direction. Several factors affect these wet lengths: (1) contact angles, (2) draw-down ratio, (3) slot-to-drum angle, (4) slot-to-drum distance, (5) pinning traction, (6) extrudate (die) swell, especially due to any viscoelasticity of the melt.[13] In addition, transient lip wetting during startup or process upsets can change the wetting characteristics of the lips and cause additional steady-state wetting.

A small vacuum (0.25 kPa = 1″ H_20) was next imposed on the lower free surface in addition to the electrostatic force. Figure 7 shows the initial and final states. There is now a major change of the free curtain both in shape and position. There are no inflection points, both free surfaces are concave and monotonic in curvature, and the contact

Table 3. Parameter Values of Case s-s #2

Parameters	Symbol	Base value
Cast film thickness	H_1	1.68 mm
Die-lip opening	H_0	3.12 mm
Die-to-drum vertical distance	d	16 mm
Pinning-wire to die exit horizontal distance	d_w	37.5 mm
Drum speed	V_w	0.208 m s^{-1}
Die entry mean velocity	V_d	0.112 m s^{-1}
Maximum electrostatic traction	P_{max}	1 kPa
Viscosity	μ	137.7 Pa s
Density	ρ	1200 kg m^{-3}
Surface tension	σ	20 mN m^{-1}
Dynamic contact angle	θ_d	179.9°
Upstream die static contact angle	θ_{S1}	20°
Downstream die static contact angle	θ_{S2}	20°
Slot-drum angle	α	94.6°
Drum-gravity angle	β	−85.4°
Die cutback angle 1	δ	90°
Die cutback angle 2	γ	90°

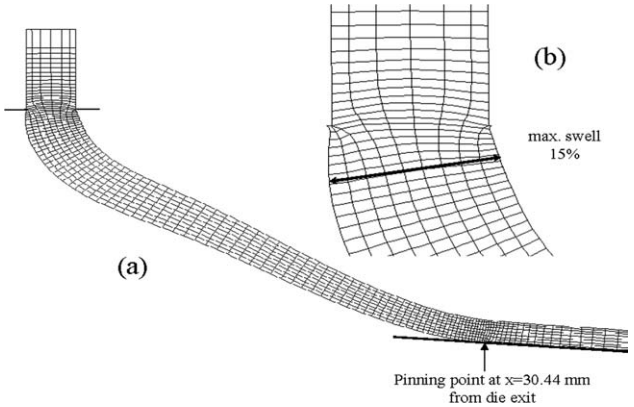

Figure 8. Finite element mesh of computed steady state of the non-horizontal round drum case (s-s #2).

(a) Full domain; (b) detail in the die exit region.

point C is brought much further upstream at $x_C = 16.64$ mm. However, the upstream and downstream wet lengths in this case do not seem to be affected much by this level of applied vacuum.

Nonhorizontal round drum substrate

A second steady state (s-s #2) was calculated taking into account the correct slot-drum angle at the attachment point and a different electrostatic force (see Table 3). The electrostatic force here was taken normal to the free surface (like a pressure) rather than normal to the drum. It is assumed to be of Gaussian shape corresponding to $c = 0.25$ in Eq. 10 (the maximum P_{max} was taken to be 1 kPa), while the dynamic contact line pins at a location of $x_C = 30.44$ mm from the die exit (the x-axis origin is at the upstream slot tip). For this case, the dimensionless parameters are: Re = 0.015, Ca = 756, St = 0.186. Again, these numbers indicate that inertia and surface tension effects are not very important (very viscous flows), while gravity does play now a bigger role in the domain at hand.

Figure 8a shows the free surface profile and finite element mesh of s-s #2 at the base parameter set of Table 3. Again, the main feature of this flow is an inflection point on the lower free surface. Figure 8b shows a detail around the slot exit. Because of the rearrangement of the velocity profile

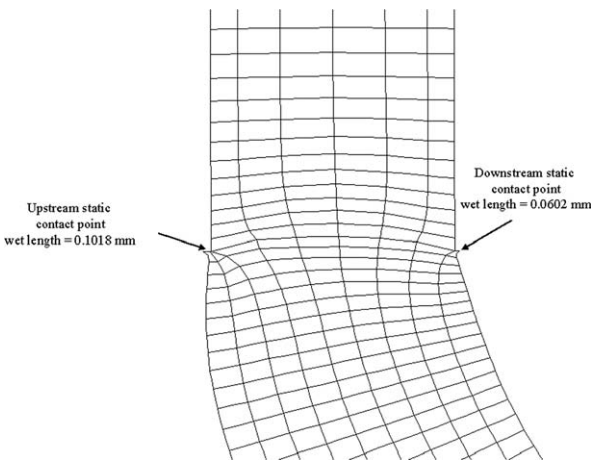

Figure 9. Blown-up finite element mesh of computed s-s #2 in the die exit region.

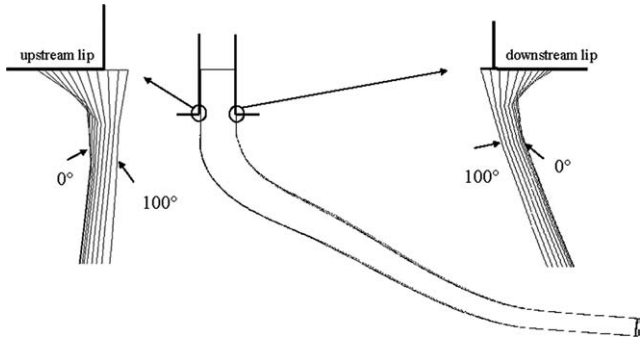

Figure 10. Free surface profiles for varying the static contact angle θ_S from 0 to 100° and details in the vicinity of the static contact lines (s-s #2).

from almost parabolic inside the die into a plug-like as the material flows out of the die, there appears the phenomenon of extrudate swell.[13,22,23] The maximum extrudate swell was predicted to be 15%. This is different from the base-case (Re = St = 0, Ca = ∞) extrudate swell of 1.190 ± 0.002 in planar dies.[22] However, here due to the pinning force applied on the curtain, the base-case swelling is modified due to the surface forces (surface tension, hence Ca, and surface traction P) applied on the free boundary, which cause bending. The maximum extrudate swell was predicted to be 15%. The upstream wet length h_S was found to be 0.1018 mm and the downstream one 0.0602 mm (Figure 9). Again, a distinctly nonuniform lip-wetting phenomenon occurs.

Static contact angle variations

Starting from the base case s-s #2 at the parameter set given in Table 3, 2-D steady states were computed for varying the static contact angle, θ_S, and die-lip opening, H_0, using a higher-order continuation scheme by means of the differential-algebraic-system-solver (DASSL).[24,25] DASSL was slightly modified to allow steady-state continuation by substituting the continuation parameter of interest (static contact angle, die gap) for "time." DASSL does higher-

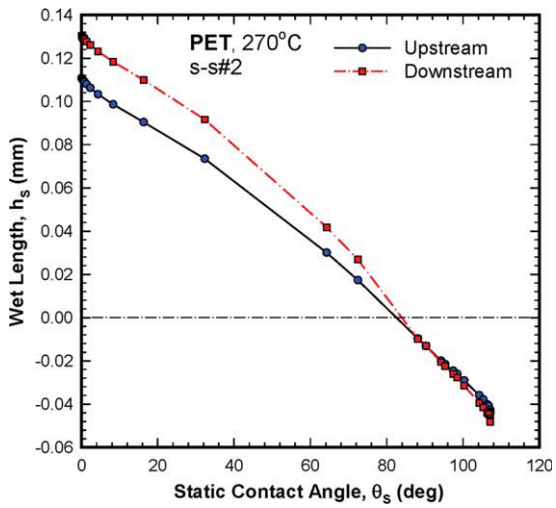

Figure 11. Upstream and downstream static contact line locations for varying the static contact angle θ_S from 0 to 107° (s-s #2).

[Color figure can be viewed in the online issue, which is available at wileyonlinelibrary.com.]

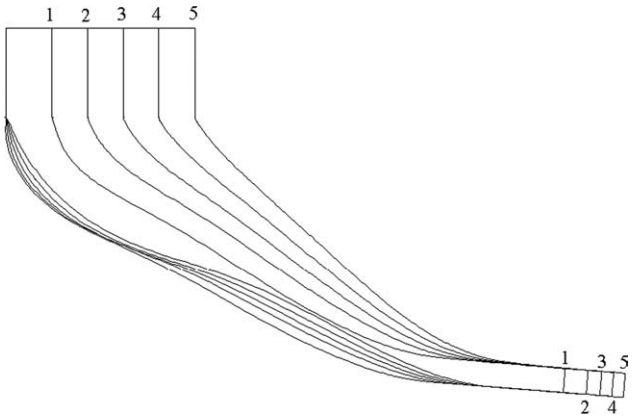

Figure 12. Free surface profiles for varying the die gap H_O from 3.12 to 15.44 mm (s-s #2). The numbers 1–5 correspond to the five cases studied.

order interpolation (backward difference of degree 2–5) and picks the degree that maximizes the time (parameter) step.

Two continuation runs were performed for varying the static contact angle taken to be the same on the upstream and downstream die lands, one for values above the base case value (20–107°) and one below (0–20°). The combined results are shown in Figures 10 and 11.

Figure 10 shows the free surface profiles for static contact angles ranging from 0 to 100°. The locations of the two static contact lines on the die lips are predicted by the analysis. Evidently, there is little change in the macroscopic flow and the wetting as the contact angle changes. The magnified views (by 81 times) of the free surface profiles in the vicinity of the upstream and downstream contact lines (again, the FIPOST post-processor substitutes the quadratic functions used for the free-surface parameterization with piecewise linear functions and makes the apparent contact angle in the figures seem greater than 0°).

Figure 11 plots the computed wetted lengths as functions of the imposed static contact angle. Evidently, from these

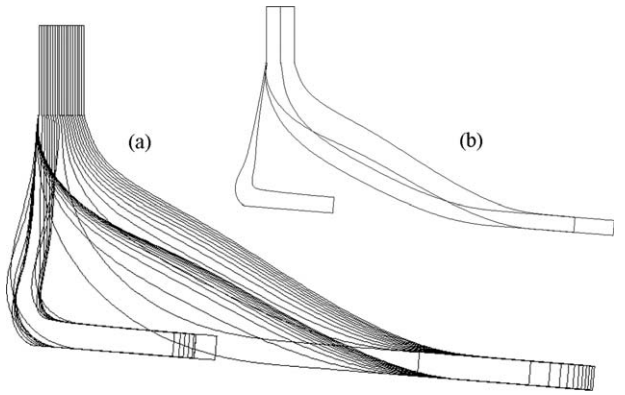

Figure 14. Free surface profiles for varying the die gap from 3.12 to 0.033 mm in s-s #2: (a) 20 states, (b) three states, equidistant.

two figures there is very little wetting of the lips. This is probably due to the high melt viscosity and the strong extension of the melt curtain by the drum, causing a contraction in the thickness direction and a lip dewetting tendency manifested as little change of the wetting line positions with contact angle. The contact lines essentially remain pinned at the corners. However, an interesting observation arises: for static contact angles larger than 84°, negative wetted lengths are predicted. This is obviously a nonphysical artifact of the fact that the current version of the model does not allow for dewetting of the surfaces of the feed slot. Of course the static contact angles are believed to be much smaller (10–20°). For future calculations, the model will be extended to account for such dewetting, which may be the main cause of streaks.

Because of the high melt viscosity, the capillary number of the flow is high as surface forces are much less important than viscous forces. The effect of surface forces is therefore confined to a length invisibly small so as not to affect the "apparent" static contact angle. For this reason, future calculations will be performed with the static contact angles

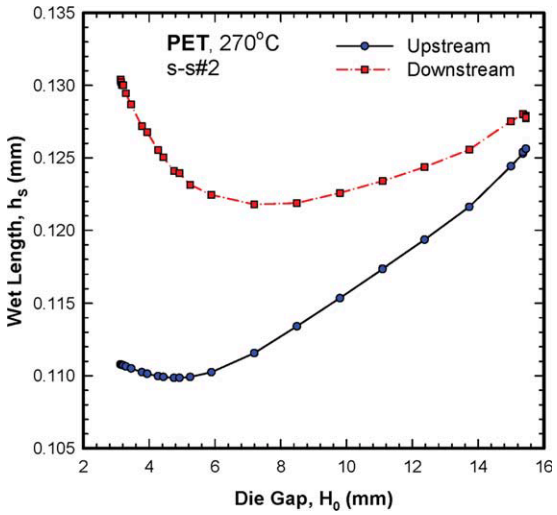

Figure 13. Predicted upstream and downstream static contact line locations for varying the die gap H_0 from 3.12 to 15.44 mm (s-s #2).

[Color figure can be viewed in the online issue, which is available at wileyonlinelibrary.com.]

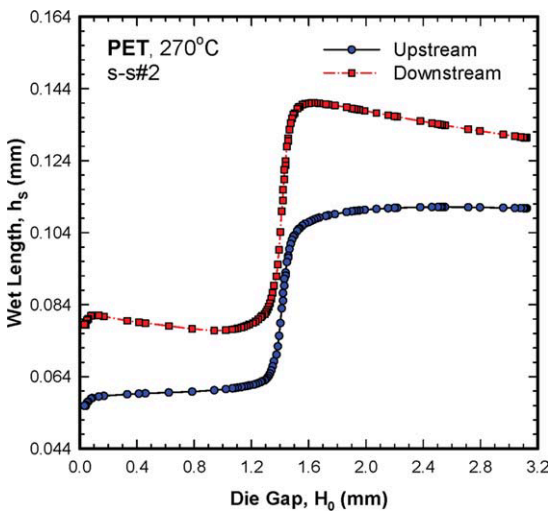

Figure 15. Predicted upstream and downstream static contact line locations for varying the die gap from 0.033 to 3.12 mm in s-s #2.

[Color figure can be viewed in the online issue, which is available at wileyonlinelibrary.com.]

imposed as "natural" rather than "essential" conditions, i.e., through forces in the momentum balances rather than imposed explicitly.

Die gap variations

In a second set of runs, the die gap was varied below and above the base case value of 3.12 mm. Figure 12 shows the computed steady state free surface profiles for varying the die gap in the range of 3.12–15.44 mm. Again, there is little change in the wetted lengths. Figure 13 plots the wetted lengths as functions of the die gap in the same range. Figure 14b shows the free surface profiles for varying the die gap in the range of 3.12–0.033 mm (three equidistant states) and Figure 14a is a more refined version (20 states). Figure 15 plots the two wetted lengths as functions of the die gap.

An interesting observation can be made from these three figures: for die gaps around half of the initial ($\sim$1.524 mm), a drastic rearrangement of the liquid curtain occurs. It suddenly changes from a downstream-drawn state by the casting drum to one in which the curtain issuing from the feed slot buckles in the upstream direction. At the same time, the two wetted lengths are reduced to about half their original values of 0.14 and 0.11 mm to 0.06 and 0.08 mm, respectively. Such a region of die-gap should be avoided in practice as the flow is expected to be sensitive to external disturbances.

Conclusions

A finite element model of the film-casting process with wire pinning was developed and used to predict the sensitivity of the static wetting line locations to the imposed static contact angle and die gap values. It was found that while the contact angle has a small effect on the extent of die-lip wetting within the parameter ranges examined, there is a considerable chance that the feed slot surfaces can be dewetted as was shown in Figure 10. This seems to be the greatest danger for causing streaks rather than excessive wetting of the die lands.

Several other factors can affect these wetted lengths: (1) upstream and downstream lip extensions; (2) slot-drum angle; (3) slot-drum distance; (4) location of electrostatic pinning wire and magnitude of electrostatic force; and (5) extrudate (die) swell, especially due to any viscoelasticity of the melt. In addition, transient lip wetting during startup or process upsets can change the wetting characteristics of the lips and cause additional steady-state wetting. These effects can be considered using continuation schemes in the corresponding parameter domains.

Also important is the effect of viscoelasticity as was shown in our previous studies for PET, where a Phan-Thien/Tanner model was used to fit the rheology of the melt.[9,10] However, the coupling of the present scheme with viscoelasticity is not trivial and will be the subject of a future study.

Acknowledgments

Financial support from the Natural Sciences and Engineering Research Council (NSERC) of Canada, the National Technical University of Athens (NTUA) of Greece.

Literature Cited

1. Dobroth T, Erwin L. Causes of Edge Beads in Cast Films. *Polym Eng Sci*. 1986;26:462–467.
2. Pakula T, Fischer EW. Instabilities of the deformation process in cold drawing of poly(ethylene terephthalate) and other polymers. *Polym Sci Polym Phys Ed*. 1981;19:1705–1726.
3. Petrie CJS, Denn MM. Instabilities in polymer processing. *AIChE J*. 1976;22:209–236.
4. Barq P, Haudin JM, Agassant JF, Roth H, Bourgin P. Instability phenomena in film casting process. *Intern Polym Proc*. 1990;4: 264–271.
5. Anturkar NR, Co A. Draw resonance in film casting of viscoelastic fluids: a linear stability analysis. *J Non-Newtonian Fluid Mech*. 1988;28:287–307.
6. Yamada T, Matsuo T, Kase S, Tosa T. Theoretical analysis of film casting process with a pinning device under steady state. *J Polym Eng*. 2008;28:287–310.
7. Yamada T, Matsuo T, Kase S, Tosa T. Theoretical analysis of film casting process with a pinning device under a transient state. *J Polym Eng*. 2008;28:311–347.
8. Christodoulou KN, Kistler SF, Schunk PR. *Advances in computational methods for free-surface flows*. In Schweizer PM, Kistler SF, editors. *Liquid Film Coating—Scientific Principles and Their Technological Implications*, New York: Chapman and Hall, 1997: 297–357.
9. Hatzikiriakos SG, Heffner G, Vlassopoulos D, Christodoulou KN. Rheological characterization of PET resins using a multimode Phan-Thien-Tanner constitutive relation. *Rheol Acta*. 1997;36:568–578.
10. Christodoulou K, Hatzikiriakos SG, Vlassopoulos D. Stability analysis of film casting for PET resins using a multimode Phan-Thien-Tanner constitutive equation. *J Plast Film Sheeting*. 2000;16: 312–332.
11. d'Halewyn S, Agassant JF, Demay Y. Numerical simulation of the cast film process. *Polym Eng Sci*. 1990;30:335–340.
12. Barq P, Haudin JM, Agassant JF. Isothermal and anisothermal models for cast film extrusion. *Intern Polym Proc*. 1992;7:334–349.
13. Debbaut B, Marchal JM, Crochet MJ. Viscoelastic effects in film casting. *Z Angew Math Phys* 1995;46; S679–S698.
14. Beaulne M, Mitsoulis E. Numerical simulation of the film-casting process. *Intern Polym Proc*. 1999;14:261–275.
15. Weatherburn CE. *Differential Geometry of Three Dimensions*. Cambridge: Cambridge Universtiy Press, 1927.
16. Bathe KJ. *Finite Element Procedures in Engineering Analysis*. Englewood Cliffs, NJ: Prentice Hall, 1982.
17. Zaretsky MC, Benson JE. Improved electrostatic pinning using a biased conductive shield. *J Electrostat*. 1977;40:735–740.
18. Christodoulou KN, Scriven LE. Discretization of free surface flows and other free boundary problems. *J Comput Phys*. 1992;99:39–55.
19. Georgiou GC, Boudouvis AG. Converged solutions of the Newtonian extrudate-swell problem. *Int J Numer Meth Fluids*. 1999;29:363–371.
20. Mitsoulis E, Hatzikiriakos SG, Christodoulou K, Vlassopoulos D. Sensitivity analysis of the bagley correction to shear and extensional rheology. *Rheol Acta*. 1998;37:438–448.
21. FIPOST. *A finite element post-processor for FIDAP®, FIDAP Manual*, Fluent Inc., 2011. Available at: www.ansys.com.
22. Tanner RI. *Engineering Rheology*, 2nd ed. Oxford: Oxford University Press, 2000.
23. Mitsoulis E. Extrudate swell of Boger fluids. *J Non-Newtonian Fluid Mech*. 2010;165:812–824.
24. Petzold LR. *A Description of DASSL: A Differential/Algebraic System Solver*. SAND82–8637, Livermore, CA: Sandia National Laboratories, 1982.
25. Petzold LR, Loetstedt P. Numerical solution of nonlinear differential equations with algebraic constraints II: practical implications. *SIAM J Sci Stat Comput*. 1986;7:720–733.

Manuscript received May 16, 2011, and revision received July 1, 2011.